Contrib. Plasma Phys. **44**, No. 5-6, 536 – 541 (2004) / **DOI** 10.1002/ctpp.200410076

Two-Dimensional Kinetic and Three-Dimensional Fluid-Radiation Transport Simulations of Plasma Display Panel

S. S. Yang[1], **J. K. Lee**[*1], **S. W. Ko**[1], **H. C. Kim**[1], and **J. W. Shon**[2]

[1] Department of Electronic and Electrical Engineering, Pohang University of Science and Technology, Pohang 790–784, S. Korea

[2] Lam Research Corporation, 4650 Cushing Parkway, CA 94538, U.S.A.

Received 16 March 2004, accepted 16 March 2004
Published online 27 August 2004

Key words Plasma display panel, ion angle distribution, optimization.
PACS 52.65.Ce, 52.75.-d

Using fluid and kinetic simulation codes, we investigated ion angle distributions in a PDP cell. We also compared our fluid simulation results with experimental data to prove the accuracy of our codes and suggested new PDP cell structure. Kinetic simulation results shows that most ions impinge on the MgO surface at the cathode region with the incident angles in the range of $10^{\circ}\sim30^{\circ}$. Our simulation results from 2-D and 3-D fluid codes showed good agreements in the distribution of excited Xe atom density compared to the experimental data measured by laser absorption spectroscopy. Using these fluid codes, we suggested Front Address PDP cell structure. This structure has address electrode on the upper substrate and shows the improvement of luminous efficiency about 2 times in comparison with conventional model because of the arch-shaped long discharge path between two sustain electrodes.

1 Introduction

Plasma display panels (PDPs) are the leading display device with the diagonal in 40∼70 inch range. The technology of PDP has been developed rapidly for a decade and recently PDP TV with diagonal length over 70 inches has been produced. PDPs have more advantages than other displays like cathode ray tubes (CRTs), liquid crystal displays (LCDs), and projection displays in the aspects of screen size, thickness, weight, and wide view angle [1]. However, there are several issues to be solved to compete with the other displays. Low luminous efficiency and high power consumption have been the important problems for a long time. Image quality, contrast, driving method, and dependence on temperature are the main issues for PDP maker. Especially, to improve the efficiency and to reduce the consumed power, we should understand the fundamental discharge mechanism of a PDP cell. Some experiments presented useful information on discharge behavior and characteristics from the measurement of ultraviolet (UV) or infrared (IR) emission. Direct or indirect access to plasma discharge in experiment has many limitations due to the small cell size and short discharge time. Therefore, numerical simulation has been very useful for investigating the plasma discharge behavior producing the various data such as spatio-temporally resolved plasma density, potential, electric field, and wall charge distributions. In addition, luminance, discharge efficiency, and luminous efficiency can be obtained from the calculation of UV emission. For this purpose, we have developed two- and three-dimensional fluid simulation codes with the self-consistent radiation transport to suggest new PDP cell designs with high luminous efficiency [2–4, 16, 17]. To investigate the discharge mechanism, we have also used kinetic and fluid codes.

In this paper, we introduce several PDP simulation results obtained with fluid and kinetic codes. Section 2-1 contains the kinetic simulation results on ion angle and energy distributions on MgO surface at the cathode region. The comparison of fluid simulation with experimental data is also presented in Sec. 2-2. In section 2-3, we describe the advantages of 3-D fluid simulation code in comparison with 2-D fluid code and show the examples of a new PDP cell design using 3-D fluid simulation. Section 3 contains the summary of our works.

* Corresponding author: e-mail: jkl@postech.ac.kr, Phone: +82 54 279 2083, Fax: +82 54 279 2903

2 PDP simulation results

2.1 Ion angle and energy distributions

The secondary electron emission coefficient (SEEC) is an important parameter for understanding the discharge mechanism in a PDP cell. There have been many experiments and theoretical approaches to find the SEEC of MgO or other protective materials [5–7]. However, these experiments or theories present different SEEC values. We have already estimated the effective SEEC (γ_{eff}) of MgO by comparing the Paschen curves from simulation with experimental data for discharge breakdown in a PDP cell and described γ_{eff} as a function of E/p [8]. Generally, in experiment, the ion beam system is used to measure the SEEC from target materials. However, the energies of the ion beam in most experiments are much higher than ion energies at the cathode region in kinetic simulation. Using the kinetic simulation with ion charge exchange and scattering collisions included, we found that most ion energies in the cathode sheath were below 50eV [9]. The incident angle of the ion beam is perpendicular to the target material surface. In a PDP system, the gas pressure is very high and charge exchange collisions between ions and neutrals occur frequently at the sheath region of the cathode. As a result, ions at the cathode region cannot have high energy compared to the sheath voltage drop. Therefore we estimated the incident angles of ions impinging on the MgO surface to be higher than 0°. However, the observation of incident angles in a real PDP cell is not easy. The particle velocity, energy, and incident angle data from kinetic code are very useful to investigate the fundamental discharge mechanism like striation phenomenon in a PDP cell [10, 11]. Therefore we investigated the incident angle distributions of ions on the MgO surface using 2-dimensional kinetic code (XOOPIC) [12, 13]. There has been no report about ion incident angle distribution on the cathode surface. As kinetic simulation needs very large simulation time, we simulated only a short time period [13].

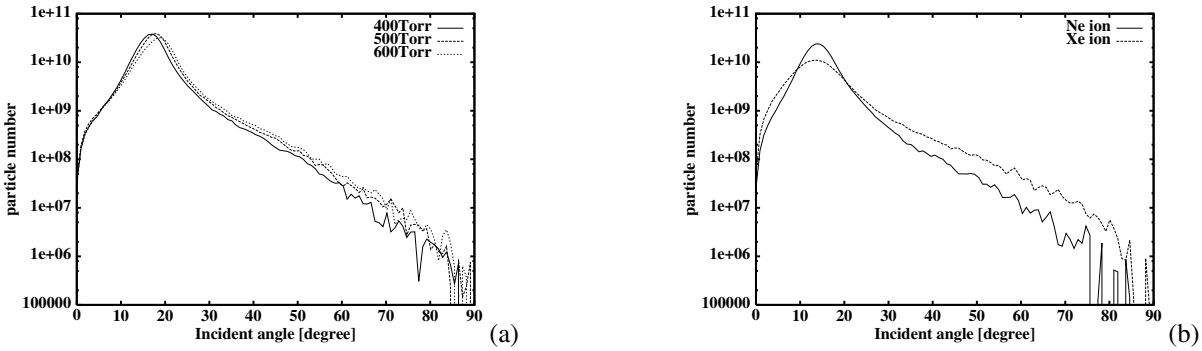

Fig. 1 Ion angle distributions in (a) pure Ne with pressure variation and (b) Ne-Xe(4%) mixture gas with gas pressure of 500Torr.

Figures 1(a) shows the incident angle distributions of Ne ions in pure Ne on the MgO surface at the cathode with pressure variation. These data are integrated until the total ion number has maximum value in space. In case of pure Ne, the incident angle for the largest particle number is about 18° in the pressure of 500Torr. 90% of Ne ions at MgO surface have the incident angles in the range of 9°∼27°. Energetic ions over 20eV are also distributed in the range of 10°∼30° and ions with incident angles over 30° have very low ion energy near the MgO surface. When the gas pressure is changed from 400 to 600Torr, the incident angle for the largest particle number is increased slightly with the reduction of energetic ions as shown in Fig. 1. Because the ion mean free path decreases with pressure increment and charge exchange collisions between ions and neutrals are dominant at the cathode sheath, the number of energetic ions is also reduced. When discharge spreads from the anode to the cathode in a PDP cell, due to positive charge accumulation and electric field variation at MgO surface of the cathode region, the hitting point of many ion particles also moves from inside to outside region of the cathode. However, the incident angle region of the large particle number still remains in the range of 18°∼20°. Figure 1(b) shows the Ne and Xe ion angle distributions for Ne-Xe(4%) with gas pressure of 500Torr. The incident angle for the largest particle number for Ne and Xe ions is reduced compared to that for pure Ne case. 90% of Ne and Xe ions have the incident angles of 7°∼21° and 3°∼25°, respectively. Ion angle distribution of Xe ions is broader than that of Ne ions.

2.2 Comparison of simulation with experiment

To confirm the accuracy and reliance of our fluid simulation codes, we compared our 2-D and 3-D simulation results with experimentally measured excited Xe species in a PDP cell [13]. Although, in experiment, direct access and diagnostics of discharge in a PDP cell have many restrictions, Tachibana et al. observed the spatio-temporal behavior of excited Xe atoms by using the laser absorption spectroscopy technique in a real PDP system [14, 15]. We have focused our comparison on the spatio-temporal behavior of excited Xe atom density and the total number of metastables ($Xe^*(^3P_2)$). To do this comparison, we took into account the effect of radiation transport and the molecular ions like Xe_2^+, Ne_2^+, and $NeXe^+$ in our 2-D and 3-D fluid simulation codes. To describe the resonance radiation transport of UV emitted from $Xe^*(^3P_1)$, we use the modified Holstein's equation instead of the effective trapping factor method [16,17]. Molecular ions are generated by three-body collisions and Penning ionization of metastable Ne atoms or metastable Ne molecules. Adding the radiation transport model and the reactions of the molecular ions, the accuracy of simulation codes increases compared to previous codes. The gas composition used for this comparison is Xe(5%)–Ne with gas pressure of 500Torr. The SEECs of MgO layer for Ne and Xe ions are 0.5 and 0.05, respectively.

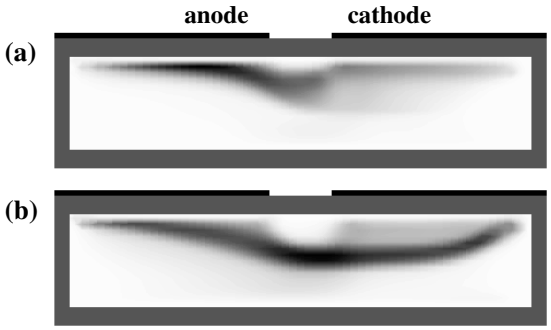

Fig. 2 $Xe^*(^3P_2)$ density distributions in cases of sustain voltage (a) 200V and (b) 250V.

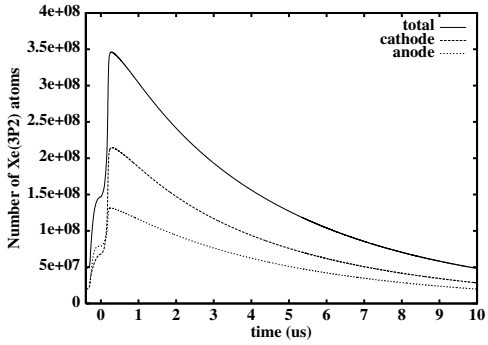

Fig. 3 Total number of $Xe^*(^3P_2)$ atoms at the anode and cathode region.

In the first comparison, to observe the driving voltage effect, we applied high voltage (250V) and low voltage (200V) to sustain electrodes with grounded address electrode during the sustaining period as mentioned in Ref. [14]. In case of low voltage, the density distribution of excited Xe atoms is very similar to that of general PDP case. When driving pulse is applied, initial discharge occurs at the inner edge region of the anode between two sustain electrodes. Although the distribution of excited Xe species density at the anode region is narrower than that at the cathode region, the local region with high density distribution appears at the anode region. However, in case of high voltage, pre-discharge occurs between the address electrode and the cathode before sustain pulse is applied to sustain electrodes. Because the address electrode is fixed to zero potential during the sustaining period, positive wall charges are accumulated on the address electrode. In addition, as high voltage was applied to the sustain electrode in previous pulse, negative wall charges are accumulated and produce the pre-discharge with the positive wall charges on the address electrode. Due to pre-discharge, the main discharge in the cathode region is stronger than that in the anode region and the arch-shaped discharge is formed between two sustain electrodes as shown in experiment [14]. Figures 2(a) and (b), which can be compared to Figs. 4 and 5 in Ref. [14], show the density distributions of $Xe^*(^3P_2)$ for low and high voltage cases, respectively. We have also compared the total number of excited Xe atoms at the anode and cathode regions as a function of time as presented in Fig. 3. Analogous to the experimental results (Fig. 6 in Ref. [14]), simulations show that the number of excited atoms at the cathode region is about 60% larger than that at the anode region. This is a very relevant value compared to the experimental results. The decay time from the peak number density to its half width is larger in our simulation (about 2.5μs) in comparison with experiment (about 2μs).

Recently, there have been many experimental attempts to improve the luminous efficiency using the address electrode during the sustaining period [15, 18–20]. Generally, the address electrodes are only used to select the specific cells during the reset and address period. They are fixed to zero potential during the sustaining period. For the second comparison, we applied two kinds of small additional pulses to the address electrode as shown in Fig. 4 to compare with the experimental results given in Refs. [15] and [20]. Figures 5(a)∼(c) show the density

distributions of $Xe^*(^3P_2)$ when three kinds of address pulses shown in Figs. 4(a)∼(c) are applied, respectively. Figure 5 can be compared to Fig. 4 in Ref. [15]. Reference [20] only shows the cross sectional observation of IR emission. The simulation domain and gas conditions are the same as those for the first comparison. In case of address pulse (b) in Fig. 4, the small pulses applied to the address electrode are synchronized with sustain driving pulses in rising time. In case of address pulse (c), the small pulses are applied to the address electrode before sustain driving pulses are applied to the sustain electrodes. When voltage applied to the address electrode is fixed to zero potential during the sustaining period, only surface discharge occurs horizontally along the upper dielectric layer as shown in Fig. 5(a). In simulation, small self-discharge can be observed in the cathode region before sustain pulse is applied. However, it is very weak and does not influence the main discharge. Considering some regions apart from MgO surface, which are not accessed by laser beam in experiment, the distribution of excited Xe atoms in simulation [13] is very similar to that in experiment [15].

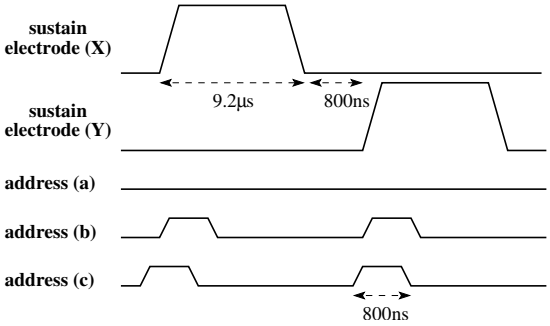

Fig. 4 Sustain pulse shape and three kinds of additional pulse shapes applied to address electrode.

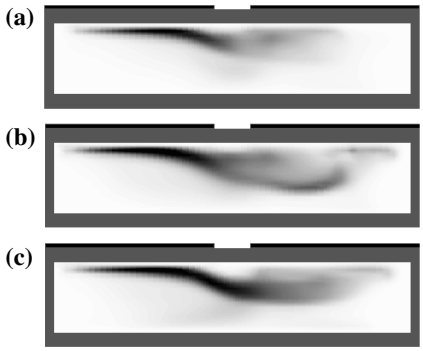

Fig. 5 $Xe^*(^3P_2)$ density distributions of three kinds of address pulses.

When additional pulses with short pulse width like address pulses (b) and (c) in Fig. 4 are applied to the address electrode, we observed the broad excited Xe density distribution at the cathode side. The discharge mechanism for address pulse (b) is different to that for address pulse (c). In case of address pulse (b), the discharge ignition is very similar to that for the case of address pulse (a) as mentioned above. When discharge spreads to the cathode side, due to the positive pulses with small amplitude, the address electrode temporally acts as the anode. High density region appears on the phosphor layer of the cathode side and excited Xe species distribute over the large region of the cathode side as shown in Fig. 5(b). As the voltage amplitude of the address electrode increases up to 60V, the discharge at the cathode region becomes stronger. Due to the increment of the generation of excited Xe species and the proximity between excited Xe species and the phosphor layer, discharge efficiency as well as luminous efficiency increases compared to the case with the address electrode fixed to zero potential. Analogous to the simulation, experimental results also show that the IR emission intensity increases and the distribution region of IR emission extends toward the address electrode when the amplitude of applied voltage is increased from 0V to 90V [20]. However, when asynchronous address pulse in Fig. 4(c) is applied to the address electrode, the pre-discharge between the address electrode and the cathode is created. Except for short time when small positive pulses are applied, the address electrode is fixed at zero potential. Therefore positive wall charges are accumulated on phosphor layer of lower substrate. If positive pulse is applied to the address electrode before main sustain pulse is applied to the anode, the potential of phosphor layer is larger than that of address electrode due to the positive wall charge. Therefore electrons are attracted from negative wall charge on the sustain electrode which will be cathode and small discharge occurs above phosphor layer before main discharge occurs at the anode side. This pre-discharge generates priming particles in the cell space and these priming particles influence the main discharge. For the same sustain voltage, the case with additional pulses on the address electrode has faster main discharge ignition than that without additional pulses. Therefore, it is possible to generate many excited Xe atoms during the rising time of the main pulse with relatively low electric field. Because the cross section of excitation is larger than that of ionization in low electric field, the generation of Ne and Xe ions is reduced compared to the case of address pulse (a). We have also changed the amplitude of pulse applied to the address

electrode. In both experiment and simulation, the total number of $Xe^*(^3P_2)$ and discharge efficiency are higher for the cases of around 60V than those for other cases as shown in experimental data [15].

2.3 PDP cell optimization using 3-D fluid code

A PDP cell should be optimized further in order to overcome major drawbacks. To do this, we utilize 2-D and 3-D fluid codes [16, 17]. Usually, 2-D code is used first for optimization. The reason for this is that most of the geometrical effects like the electrode position, gap distance, dielectric thickness, and height of barrier ribs can be considered with high precision using 2-D code. Another reason is that 3-D code is very time consuming in comparison with 2-D code. Therefore geometrical cell optimization is done with 2-D fluid code and then some models showing good efficiency are simulated with 3-D code in order to obtain detailed information [21]. However, a real PDP cell has 3-D structure, so 2-D fluid code has some limitations to analyze it elaborately.

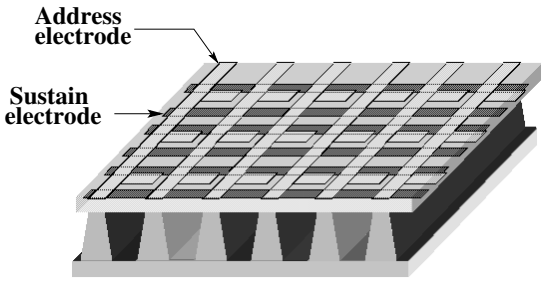

Fig. 6 Three-dimensional schematics of the Front Address model.

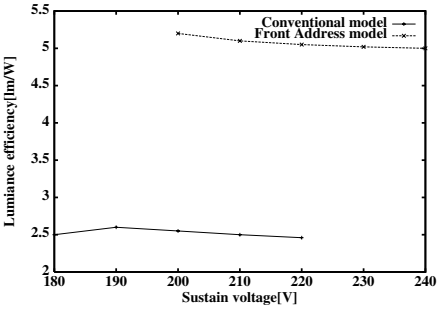

Fig. 7 Comparison of luminous efficiency between FA model and conventional model.

A conventional AC-PDP cell consists of two sustain electrodes located at the upper substrate and an address electrode situated at the lower substrate. In this subsection, we show the Front Address (FA) model which has fairly different geometry from the conventional model as shown in Fig. 6. We may imagine simply that in the FA model, the address electrode is moved to the upper substrate in comparison with the conventional model. However the FA model shows different $Xe^*(^3P_1)$ density distribution and potential profile compared to the conventional model due to a different discharge regime as presented in Fig. 8. In Figs. 8(a), (b), (c), and (d), $Xe^*(^3P_1)$ density distributions for the FA model are much longer and broader than those for the conventional case because the discharge in the FA model occurs between two sustain electrodes with a long gap. In addition, the wall charges on the address electrode help low-electric field to be formed in the central region of the discharge space. Thus, the energy by external sources is used to generate more excited species like $Xe^*(^3P_1)$ emitting 147nm UV through releasing the absorbed energy during the discharge period and $Xe^*(^3P_2)$ emitting 173nm rather than the ions. Besides, the address electrode consists of metal and transparent ITO in order to minimize the screening area when visible photons come from the window. As we can see in Fig. 6, the metal electrode part is on the barrier rib and the ITO electrode is on the discharge space. As a result, the luminous efficiency of the FA model is by the factor of 2 higher than that of the conventional model as presented in Fig. 7. Here the luminous efficiency value is relative, because general luminous efficiency of the conventional model in a real PDP cell is about 1.2 lm/W.

However, efficiency and power consumption are not independent because the efficiency is inversely proportional to the power dissipation. A lot of efforts and trials to decrease power are now under way through ITO electrode structure changes like T-shaped and Bullet-shaped sustain electrodes, keeping the original 2-D structure. Thus as long as we do not change too much the ITO structure, its 2-D effects can be kept without big changes [22, 23]. The results using our 3-D code are shown in Figs. 8 (e) and (f). As we can see, 2-D structure is the same but the sustain electrode shapes are quite different. Therefore, these results have very different distribution of Xe excited species density. In view of luminance, the White-Cross model in Fig. 8(e) shows good results because $Xe^*(^3P_1)$ density distribution is much broader than that of the Hat model presented in Fig. 8(f). Therefore more UV photon will be changed into visible light on the phosphor. To obtain good efficiency through electrode shape variation, we should know which part of the electrode contributes more to discharge and which part does not. As a matter of fact, power reduction mainly comes from the reduction in electrode area, but the imprudent reduction or removal of electrode area frequently leads to unstable discharge and bad operational

characteristics by shrink of operation margin. To evade the these side effects of the variation of electrode shape, the analysis through simulation is inevitable because the experiments have fatal restrictions in view of time and cost.

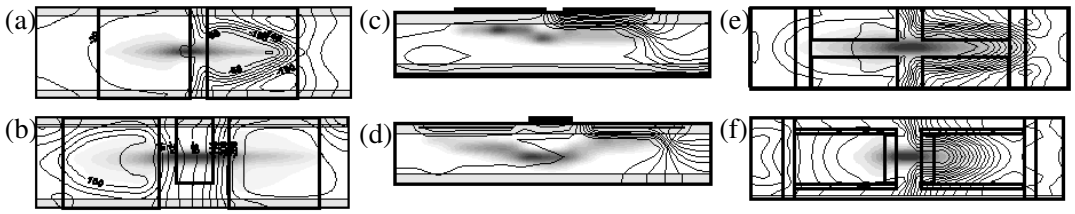

Fig. 8 $Xe^*(^3P_1)$ density and potential profiles; (a) and (c) is the top and side view of conventional model; (b) and (d) is the top and side view of FA model; (e) and (f) are the examples of sustain electrode variation.

3 Summary

We presented several PDP simulation results using 2-D or 3-D fluid and kinetic codes. From the simulation of kinetic code, we found that many ions impinging on the MgO layer at the cathode sheath have the incident angles in the range of $13^\circ \sim 20^\circ$ in pure Ne or Xe-Ne mixture gases with gas pressure of 500Torr. In comparison with experimentally measured data, the simulation shows similar characteristics for the excited Xe species density distribution and the number of excited Xe atoms. We also explain the role of address electrode when additional small pulses are applied to it using the simulation and experimental results. In view of efficiency improvement, we presented the Front Address model having the efficiency about 2 times higher than the conventional model and practical applications of the variation of electrode shape using 3-D fluid code.

Acknowledgements This work is supported in part by Korea Ministry of Information and Communication under Advanced Backbone IT Technology Development Project, LG Electronics, and by the Ministry of Education & Human Resources Development of Korea under Brain Korea 21 program.

References

[1] J. K. Lee and J. P. Verboncoeur, "Low Temperature Plasma Physics" ed. by R. Hippler et al., Berlin, Germany: Wiley-VCH, 2001, pp. 367 – 384.
[2] Y.K. Shin, C.H. Shon, W. Kim, J.K. Lee, IEEE Trans. Plasma Sci., **27**, 1366–1371 (1999).
[3] H.C. Kim, M.S. Hur, S.S. Yang, S.W. Shin, and J.K. Lee, J. Appl. Phys., **91**, 9513–9520 (2002).
[4] S.S. Yang, H.C. Kim, S.W. Ko, and J.K. Lee, IEEE Trans. Plasma Sci., **31**, 596–605 (2003).
[5] K.S. Moon, J.H. Lee, and K.W. Whang, J. Appl. Phys., **86**, 4049–4051 (1999).
[6] G. Auday, Ph. Guillot, and J. Galy, J. Appl. Phys., **88**, 4871–4874 (2000).
[7] E.H. Choi, J.Y. Lim, Y.G. Kim, J.J. Ko, D.I. Kim, C.W. Lee, and G.S. Cho, J. Appl. Phys., **86**, 6525–6527 (1999).
[8] M.S. Hur, J.K. Lee, H.C. Kim, and B.K. Kang, IEEE Trans. Plasma Sci., **29**, 861–863 (2001).
[9] Y.K. Shin, J.K. Lee, C.H. Shon, and W. Kim, Jpn. J. Appl. Phys., **38**, L174–L177 (1999).
[10] C.H. Shon and J.K. Lee, Phys. Plasmas, **8**, 1070–1080 (2001).
[11] J.K. Lee, S. Dastgeer, C.H. Shon, M.S. Hur, H.C. Kim, and S.W. Cho, Jpn. J. Appl. Phys., **40**, L528–L531 (2001).
[12] J.P. Verboncoeur, A.B. Langdon, and N.T. Gladd, Compt. Phys. Commun., **87**, 199–211 (1995).
[13] S.S. Yang, S.W. Ko, H.C. Kim, and J.K. Lee, in preparation.
[14] K. Tachibana, K. Mizokami, N. Kosugi, and T. Sakai, IEEE Trans. Plasma Sci., **31**, 68–73 (2003).
[15] Y. Shintani, J.C. Ahn, K. Tachibana, and T. Sakai, in *Proc*. The 9th IDW, 817–820 (2002).
[16] H.J. Lee, H.C. Kim, S.S. Yang, and J.K. Lee, Phys. Plasmas, **9**, 2822–2830 (2002).
[17] H.C. Kim, S.S. Yang, and J.K. Lee, J. Appl. Phys., **93**, 9516–9522 (2003).
[18] S.H. Jang, K.D. Cho, H.S. Tae, K.C. Choi, and S.H. Lee, IEEE Trans. Electron Dev., **48**, 1903–1910 (2001).
[19] H.J. Cho, B.J. Kim, J.H. Lee, and K.C. Choi, in *Proc*. The 2nd IMID, 61–64 (2002).
[20] H.J. Seo, H. Kim, D.C. Jeong, S.H. Jang, H.S. Tae, S.I. Chine, and K.W. Whang, in *Proc*. The 9th IDW, 813–816 (2002).
[21] Y.K. Shin, T.S. Hwang, S.D. Kang, H.G. Park, J.H. Ryu, H.C. Kim, S.W. Shin, and J.K. Lee, J. Information Display, **3**, 13 (2002).
[22] T. Nishio et al., in *Proc*. SID '99, 268–271 (1999).
[23] C.H. Park, S.H. Lee, D.H. Kim, Y.K. Kim, and J.H. Shin, IEEE Trans. Electron Dev., **48**, 2255–2259 (2001).